Model Predictive Control for a Full Bridge DC/DC Converter

Yanhui Xie, *Senior Member, IEEE*, Reza Ghaemi, Jing Sun, *Fellow, IEEE*, and James S. Freudenberg, *Fellow, IEEE*

***Abstract*—This paper investigates the implementation of both linear model predictive control (LMPC) and nonlinear model predictive control (NMPC) to a full bridge dc/dc converter under starting, overload, and load step change conditions. The control objective is to regulate the output voltage without violating the peak current constraint. The integrated perturbation analysis and sequential quadratic programming method is employed to solve the nonlinearly constrained optimal control problems with 300 μs sampling time. The experimental results reveal that both the LMPC and NMPC schemes can successfully achieve voltage regulation and peak current protection. The experimental results are reported and several observations, seemingly counterintuitive, are analyzed to offer insight into the use of MPC for these challenging applications.**

***Index Terms*—Full bridge dc/dc converter, integrated perturbation analysis and sequential quadratic programming (InPA-SQP), linear model predictive control (LMPC), nonlinear model predictive control (NMPC).**

I. Introduction

The full bridge dc/dc converter was initially proposed in previous studies [1] for both high power density and high power applications. It is very attractive because of its zero voltage switching, low component stresses, and high power density features [2], [3]. Moreover, its high-frequency transformer prevents fault propagation and enables a high output/input voltage ratio. Therefore, with a full bridge dc/dc converter as the power conditioning system, a low-voltage energy system can be used for high dc voltage applications, such as the dc zonal electrical distribution system of an all electric ship [4]. To investigate the voltage regulation of a full bridge dc/dc based power conditioning system, an experimental testbed was developed at the University of Michigan to support model development and to facilitate a model-based control design approach [5]. Fig. 1 depicts the configuration of the power stage of a full bridge dc/dc converter whose parameters are shown in Table I.

Several challenges arise for the dc/dc converter control design. First, the power devices of the dc/dc converters have very complicated time-varying switching behavior. Therefore, the dynamic model development of power converters is a challenge. Second, dc/dc converters as power conditioning devices typically have a wide range of operating conditions, further complicating the control design. Furthermore, the control input is bounded due to physical limitations of power converters. Finally, safe operation requirements such as peak current limits may impose additional nonlinear constraints.

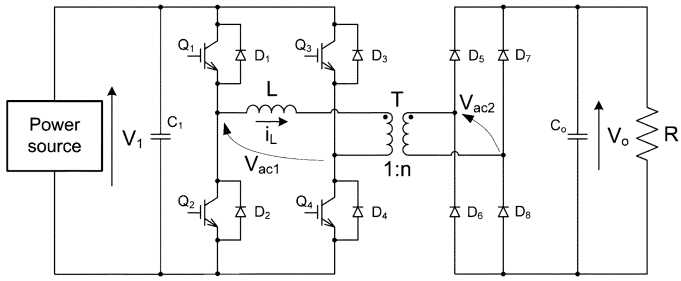

Fig. 1. Configuration of a full bridge dc/dc converter.

TABLE I
Parameters of the Testbed Prototype

Item	Parameter
Inductor L	$10.5\mu H$
Capacitor C_o	$1410\mu F$
Transformer turn ratio n	2
Switching period T	$100\mu s$
V_1 (nominal)	$60V$
Desired V_o	$80V$
Nominal load R	6.4Ω
Rated power	$1000W$

Traditionally, there are two classes of algorithms for dc/dc converter control, namely voltage-mode control and current-mode control. Voltage-mode control achieves voltage regulation through a single-loop voltage control scheme. To limit the current during transient operation to a safe operating range, the feedback control gain must be carefully chosen, otherwise an additional protection circuit has to be incorporated. In addition to a voltage feedback loop, current-mode control employs an inner inductor current feedback loop to improve performance. Performance enhancements, including superb line regulation and inherent over-current protection, can be achieved for current-mode control. However, current-mode control has a subharmonic oscillation problem when the duty ratio is greater than 0.5. Besides, this method requires inductor current sensing, which increases system cost and tends to have noise sensitivity problems. The development of advanced control algorithms, together with the increased computational power of microprocessors, enables us to deal with the control problem from a new perspective. For example, model predictive control (MPC) [6]–[8] has been implemented in power converters [9]–[11] and in an electric drive system for direct torque control [12], [13]. For the full bridge dc/dc converter under investigation, the peak current protection problem can be formulated as a constraint for an optimal control problem, which can be effectively dealt with using MPC.

In classical MPC, the control action at each time step is obtained by solving an online optimization problem with a

Manuscript received April 30, 2010; revised October 21, 2010; accepted December 13, 2010. Manuscript received in final form January 16, 2011. Date of publication February 24, 2011; date of current version December 14, 2011. Recommended by Associate Editor J. H. Lee. This work was supported in part by the US Office of Naval Research (ONR) under Grant N00014-08-1-0611 and Grant N00014-05-1-0533.

The authors are with the Department of Naval Architecture and Marine Engineering and the Department of Electrical Engineering and Computer Science, University of Michigan, Ann Arbor, MI 48109 USA (e-mail: yhxie@umich.edu; ghaemi@umich.edu; jingsun@umich.edu; jfr@eecs.umich.edu).

Color versions of one or more of the figures in this paper are available online at http://ieeexplore.ieee.org.

Digital Object Identifier 10.1109/TCST.2011.2107575

given cost function. However, solving an optimization problem is often computationally demanding, which contributes to the fact that most of the successful applications have been found for systems with slow dynamics and abundant computational power. For systems with fast dynamics, explicit MPC [16] has been proposed that pre-computes the optimal solutions and stores them for online lookup. Explicit MPC has been implemented for fast dynamic applications with a millisecond order time constant [17]. The major challenge of implementing explicit MPC is that the number of entries in the lookup table increases exponentially as the length of the horizon increases. Moreover, in explicit MPC, the nonlinear constraint is addressed using a piecewise affine approximation. As such, the size of the lookup table increases as the demand for accuracy of approximation increases. Consequently, application of explicit MPC is limited to small problems with low dimensions [18].

To extend the applicability of MPC to broader classes of systems with fast dynamics, a novel numerical optimization algorithm is developed to improve computational efficiency [19], [20]. This algorithm is referred to as the integrated perturbation analysis and sequential quadratic programming (InPA-SQP) solver. It combines the computational advantages of perturbation analysis and optimality of the SQP solution by treating the optimization problem at time k as a perturbed problem at time $k-1$. This combination can significantly improve computational efficiency and is particularly useful for MPC, where an optimal control problem must be solved repeatedly over the receding horizon. It is worthwhile to point out that the InPA-SQP algorithm can be applied to solve the MPC optimal control problem for nonlinear systems with mixed state and control input constraints.

Besides the InPA-SQP algorithm, other computationally efficient algorithms have been proposed. For example, [21] exploits the information of previous iterations in the SQP approach and the algorithm has been applied to control systems in the order of milliseconds [22]. However, this algorithm requires computation time of order $N^{2.7}$, N being the length of horizon. In comparison, the required computation time to calculate each iteration of InPA-SQP is of order N, making it an ideal candidate for the MPC implementation for power converters.

This paper is concerned with the closed-loop system performance of the MPC schemes for a full bridge dc/dc converter. The control objective is to regulate the output voltage without violating the peak current constraint. The voltage regulation is formulated as MPC problems using a linear and nonlinear model, respectively, to predict the future plant behavior. The peak current protection requirement is formulated as a nonlinear constraint. Since the full bridge dc/dc converter has a wide operating range, an offset-free algorithm [14], [15] is adopted to eliminate the steady-state error for the linear model predictive control (LMPC) scheme. To achieve 300 μs sampling time and to handle the nonlinear constraint, the InPA-SQP method is employed to solve the constrained optimal control problem. The InPA-SQP solver can significantly improve computational efficiency while effectively handling the nonlinear constraints, making the implicit MPC feasible for a power electronics system with very fast dynamics. The experimental results reveal that both the LMPC and nonlinear model predictive control (NMPC) algorithms can successfully achieve voltage regulation and peak current protection. Note that it is not our intention to compare the two schemes. Instead, it is of interest to report several observations that are seemingly counterintuitive at the first glance for the two schemes. Those observations suggest that: 1) longer prediction horizon does not guarantee better performance for both the LMPC and NMPC schemes; and 2) LMPC does not necessarily have shorter computational time than the nonlinear model-based counterpart.

The rest of this paper is organized as follows. In Section II, the inductor peak current constraint of the full bridge dc/dc converter will be presented. Section III is devoted to an observer design for states and parameter estimation using a large signal dynamic model. Section IV focuses on MPC problem formulation. Experimental results will be presented in Section V, followed by conclusion in Section VI.

II. Inductor Peak Current Constraint

The full bridge dc/dc converter is typically modulated by phase-shift modulation signals. By shifting the phase between the two half bridges, different combinations of $V_{\rm ac1}$ and $V_{\rm ac2}$ can be applied to shape the current i_L and consequently to manipulate the power flow.

Depending on the waveform of the inductor current i_L, the full bridge dc/dc converter can operate in one of two modes: the discontinuous-conduction-mode (DCM) and continuous-conduction-mode (CCM). For a full bridge dc/dc converter operating with DCM [5], the peak current $i_L(t_0+(\beta T)/(2))$ can be calculated as

$$i_L\left(t_0+\frac{\beta T}{2}\right)=\frac{(nV_1-V_o)\beta T}{2nL} \tag{1}$$

where β is the phase shift and other variables are defined in Table I.

Similarly, the peak current $(i_L(t_0+(\beta T)/(2)))$ for CCM can be calculated as

$$i_L\left(t_0+\frac{\beta T}{2}\right)=\frac{(nV_1-V_o)(V_o+nV_1\beta)T}{8nLV_1}. \tag{2}$$

The operating mode of the dc/dc converter is determined by V_1, V_o, and β. For different combinations of V_1 and V_o, the phase-shift boundary line $L_{\beta b}$ between the CCM and DCM can be calculated as follows:

$$L_{\beta b}=\left\{(\beta,V_1,V_o)\,|\,\beta=\frac{V_o}{nV_1}\right\}. \tag{3}$$

Moreover, let $i_{\rm pk}$ denotes the maximum tolerable peak current of the converter. Using (1) and (2) , one can determine the limits on the phase shift to avoid over-peak-current. The phase-shift constraint curves $L_{\beta d}$ and $L_{\beta c}$ for DCM and CCM, respectively, can be calculated from (2) and (1) as follows:

$$L_{\beta d}=\left\{(\beta,V_1,V_o)\,|\,\beta=\frac{2nLi_{\rm pk}}{T(nV_1-V_o)}\right\} \tag{4}$$

$$L_{\beta c}=\left\{(\beta,V_1,V_o)\,|\,\beta=\frac{8Li_{\rm pk}}{T(nV_1-V_o)}-\frac{V_o}{nV_1}\right\}. \tag{5}$$

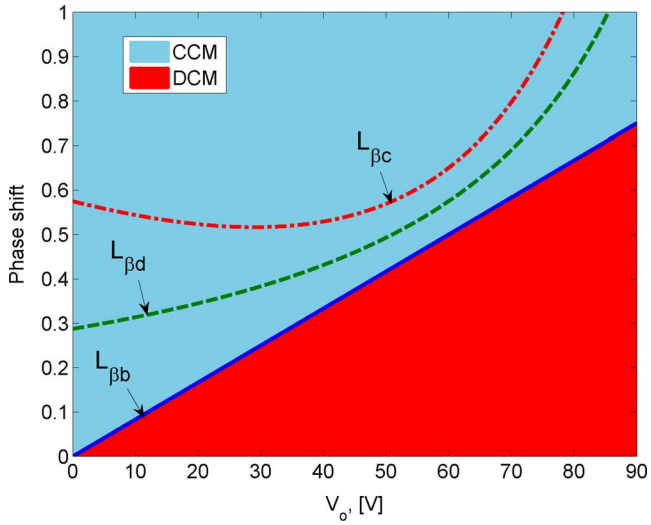

Fig. 2. DCM/CCM boundary line $L_{\beta b}$ and peak current constraint curves $L_{\beta d}$ and $L_{\beta c}$ for $V_1 = 60$ V and $i_{\rm peak} = 75$ A.

Fig. 2 shows the phase-shift boundary line $L_{\beta b}$ and the peak current constraint curves $L_{\beta d}$ and $L_{\beta c}$ for $V_1 = 60$ V and $V_o = 0$ V $\sim$ 90 V. Note that: 1) the full bridge dc/dc converter operates with the CCM if the phase shift is larger than the corresponding boundary value; and 2) the peak current constraint curves $L_{\beta d}$ and $L_{\beta c}$ are calculated using (5) and (4) for $i_{\rm pk} = 75$ A. For our system with a nominal output power of 1000 W, the phase shift at the nominal operating point is 0.62 which is smaller than the boundary value 0.67. Therefore, the converter operates with the DCM at steady state for the nominal output power. From Fig. 2, the DCM peak current constraint curve $L_{\beta d}$ is always above the boundary line $L_{\beta b}$, so the peak current constraint will not be violated if the power converter operates with DCM at steady state. However, for the cases of start-up and overload, the power converter operates at CCM, where the CCM peak current constraint may be violated. Therefore, an active constraint enforcement mechanism needs to be incorporated to protect the converter.

III. Nonlinear Dynamic Model and Observer

For the dynamic model of the full bridge dc/dc converter derived in [5], the implementation of advanced control strategies requires the values of the load resistance R and the average current $\bar{i}_L$. The load resistance R is typically a bounded unknown parameter. However, it is necessary to estimate this parameter for both the LMPC and NMPC schemes. Meanwhile, if we use a current sensor to obtain $\bar{i}_L$, the current sensor must have high bandwidth to accurately reconstruct the current signal. To overcome this drawback, we treat the load resistance R as a state and use a nonlinear observer to estimate R and $\bar{i}_L$ while keeping $\bar{V}_o$ as the only measured variable. Based on the dynamic model derived in [5], the high-gain nonlinear observer is expressed as follows:

$$\frac{d\hat{\bar{i}}_L}{dt} = \frac{\beta V_1}{L} - \frac{4\hat{\bar{i}}_L \hat{\bar{V}}_o}{\beta T(nV_1 - \hat{\bar{V}}_o)} + H_1(y - \hat{y}) \tag{6}$$

$$\frac{d\hat{\bar{V}}_o}{dt} = \frac{\hat{\bar{i}}_L}{nC_o} - \frac{\hat{\bar{V}}_o}{RC_o} + H_2(y - \hat{y}) \tag{7}$$

$$\frac{dR}{dt} = H_3(y - \hat{y}) \tag{8}$$

$$\hat{y} = \hat{\bar{V}}_o \tag{9}$$

where H_1, H_2, and H_3 are the nonlinear observer gains. Based on the separation principle, we choose high observer gains to achieve fast convergence for the estimated state.

IV. MPC Formulation

This section presents the formulation of the LMPC and NMPC schemes for the full bridge dc/dc converter. The control objective is to regulate the output voltage without violating the peak current constraint. For a given inductor peak current $i_{\rm pk}$, the CCM peak current (2) must satisfy

$$\frac{(nV_1 - V_o)(V_o + nV_1\beta)T}{8nLV_1} \le i_{\rm pk}. \tag{10}$$

If we define $x = [x_1, x_2]^T = [\bar{i}_L, \bar{V}_o]^T$ and $u = \beta$, (10) can be rewritten in terms of the state variables and control input as

$$E_1(x, u) \le 0 \tag{11}$$

where

$$E_1(x, u) = \frac{(nV_1 - x_2)(x_2 + nV_1 u)}{8nLV_1} - \frac{i_{\rm pk}}{T}.$$

Then, the peak current protection requirement can be formulated as a mixed states and control input constraint for both LMPC and NMPC schemes that will be described in the following two sections.

A. Linear Offset-Free MPC Formulation

The dynamic system can be easily linearized at the nominal operating point ($V_o = 80$ V and $P_o = 1$ kW) with nominal values $x^o = [25, 80]^T$ and $u^o = 0.62$. Letting $\tilde{x}_1 = \bar{i}_L - 25$, $\tilde{x}_2 = \bar{V}_o - 80$ and $\tilde{u} = \beta - 0.62$, the system can be transformed into its discrete-time version for a specific sampling time

$$\tilde{x}(k+1) = f(\tilde{x}(k), \tilde{u}(k)) = A\tilde{x}(k) + B\tilde{u}(k) \tag{12}$$

$$\tilde{y}(k) = F\tilde{x}(k) \tag{13}$$

where $A \in \mathbb{R}^{n\times n}$, $B \in \mathbb{R}^{n\times m}$, $F \in \mathbb{R}^{m\times n}$. Note that $n = 2$ and $m = 1$ for the system under investigation.

The peak current constraint (11) can be rewritten as

$$E_1(x(k), u(k)) = \frac{(nV_1 - (x_2^o + \tilde{x}_2(k)))(x_2^o + \tilde{x}_2(k))}{8nLV_1} + \frac{(nV_1 - (x_2^o + \tilde{x}_2(k)))n(u^o + \tilde{u}(k))}{8nL} - \frac{i_{\rm pk}}{T}. \tag{14}$$

Since the model represented by (12) and (13) is obtained by linearizing at a given operating point, the modeling error will lead to nonzero steady-state error for closed-loop system with conventional MPC. To eliminate the steady-state error, offset-free MPC has been developed in previous studies [14], [15].

For this application, the plant model represented by (12) and (13) can be augmented with a constant disturbance model

$$\tilde{x}(k+1) = A\tilde{x}(k) + B\tilde{u}(k) + B_d d(k) \tag{15}$$
$$d(k+1) = d(k) \tag{16}$$
$$\tilde{y}(k) = F\tilde{x}(k). \tag{17}$$

Based on the augmented model, the state and disturbance estimator can be designed as

$$\hat{\tilde{x}}(k+1) = A\hat{\tilde{x}}(k) + B\tilde{u}(k) + B_d\hat{d}(k) + H_4(-F\tilde{x}(k) + F\hat{\tilde{x}}(k)) \tag{18}$$
$$\hat{d}(k+1) = \hat{d}(k) + H_5(-F\tilde{x}(k) + F\hat{\tilde{x}}(k)) \tag{19}$$

where H_4 and H_5 are observer gains that are designed to achieve fast convergence [15].

By (15)–(17), the steady-state values of the observer states must satisfy

$$\begin{bmatrix} A-I & B \\ F & 0 \end{bmatrix} \begin{bmatrix} \hat{\tilde{x}}_s \\ \tilde{u}_s \end{bmatrix} = \begin{bmatrix} -B_d\hat{d}_s \\ 0 \end{bmatrix} \tag{20}$$

where $\tilde{u}_s$ is the steady-state input while $\hat{\tilde{x}}_s$ and $\hat{d}_s$ are steady-state values of the observed state and disturbance, respectively.

Then, the MPC online optimization problem can be formulated as follows: let $\delta\tilde{x}(k) = \tilde{x}(k) - \hat{\tilde{x}}_s$ and $\delta\tilde{u}(k) = \tilde{u}(k) - \tilde{u}_s$; at the time instant k , the state of the system, $\tilde{x}(k)$, is estimated and the following optimal control problem $P_N(\delta\tilde{x}(k))$ is solved

$$P_N(\delta\tilde{x}(k)) : V_N^*(\delta\tilde{x}(k)) = \min_{\delta\tilde{\mathrm{x}},\delta\tilde{\mathrm{u}}} \{V_N(\delta\tilde{x}(k), \delta\tilde{\mathrm{u}})\}$$
$$V_N(\delta\tilde{x}(k), \delta\tilde{\mathrm{u}}) = \sum_{j=k}^{k+N-1} G(\delta\tilde{x}(j), \delta\tilde{u}(j)) + \Phi(\delta\tilde{x}(N)) \tag{21}$$

subject to

$$\delta\tilde{x}(k+1) = A\delta\tilde{x}(k) + B\delta\tilde{u}(k) \tag{22}$$
$$\delta\tilde{x}(0) = \delta\tilde{x}(k) \in \mathbb{R}^n \tag{23}$$
$$E(\delta\tilde{x}(\cdot), \delta\tilde{u}(\cdot)) \le 0, \quad E : \mathbb{R}^{n+m} \to \mathbb{R}^l \tag{24}$$

where

$$\delta\tilde{\mathrm{u}} = \{\delta\tilde{u}(k), \delta\tilde{u}(k+1), \ldots, \delta\tilde{u}(k+N-1)\} \tag{25}$$

is the control sequence

$$\delta\tilde{\mathrm{x}} = \{\delta\tilde{x}(k), \delta\tilde{x}(k+1), \ldots, \delta\tilde{x}(k+N)\} \tag{26}$$

is the state trajectory

$$G(\delta\tilde{x}(j), \delta\tilde{u}(j)) = \delta\tilde{x}(j)^T Q_1 \delta\tilde{x}(j) + \delta\tilde{u}(j)^T W_1 \delta\tilde{u}(j), \quad j = k, k+1, \ldots, k+N-1 \tag{27}$$

and $\Phi(\delta\tilde{x}(N))$ is the penalty for the final states. $Q_1 \in \mathbb{R}^{n\times n}$ and $W_1 \in \mathbb{R}^{m\times m}$ are the corresponding weighting matrices that are used to penalize the deviations of the output and the control input from their corresponding desired values, N is the prediction horizon, and $E(\delta\tilde{x}(k), \delta\tilde{u}(k))$ is the constraint matrix and can be written as follows with $l = 3$:

$$\begin{bmatrix} \delta\tilde{u}(j) + \tilde{u}_s - (1 - u^o) \\ -\delta\tilde{u}(j) - \tilde{u}_s - u^o \\ E_1(\delta\tilde{x}(j) + \hat{\tilde{x}}_s, \delta\tilde{u}(j) + \tilde{u}_s) \end{bmatrix}. \tag{28}$$

Note that the first two components are derived because of the boundedness of the phase shift ($\beta \in [0, 1]$) and each component in (28) is bounded above by zero.

Linearized models have been successfully employed for MPC optimization for many practical applications [23]. However, the difficulty that we face in voltage regulation and peak current protection of a full bridge dc/dc converter is due to the nonlinear constraint (24). As opposed to linearization of the model of the system, linearization of nonlinear constraint can easily lead to constraint violation, and since the nonlinear constraint (24) is a hard constraint, we cannot afford any violation. Moreover, inclusion of nonlinear constraints in MPC formulation requires iterative linearization of constraints until convergence to the optimal solution. Therefore, using linearized model is not expected to provide considerable computational saving in comparison with its nonlinear counterpart. On the other hand, NMPC has two advantages over LMPC. First, the nonlinear model is much more accurate than the linearized model over a wide operating of a power converter, and therefore, there might be no need for offset-free observer design. Second, with NMPC, prediction of future is more accurate, and therefore, longer length of horizon is expected to lead to better performance. In contrast, with LMPC, longer prediction horizon can lead to larger errors in predicted states that adversely affects performance of LMPC or even can jeopardize successive feasibility of MPC strategy. These observations motivated us to seek alternative NMPC formulation, with the goal to understand the difference in implementation and to gain insight for both LMPC and NMPC for this kind of application.

B. Nonlinear MPC Formulation

The nonlinear system can be transformed into its discrete-time version for a specific sampling time

$$x(k+1) = f(x(k), u(k)) \tag{29}$$
$$y(k) = Fx(k). \tag{30}$$

The CCM peak current constraint (11) can be rewritten as

$$E_1(x(k), u(k)) = \frac{(nV_1 - x_2(k))(x_2(k) + nV_1 u(k))}{8nLV_1} - \frac{i_{\mathrm{pk}}}{T}. \tag{31}$$

Then, the MPC online optimization problem can be formulated as follows: at the time instant k, the state of the system $x(k)$ is observed and the following optimal control problem $P_N(x(k))$ is solved:

$$P_N(x(k)) : V_N^*(x(k)) = \min_{\mathrm{x,u}} \{V_N(x(k), \mathrm{u})\}$$

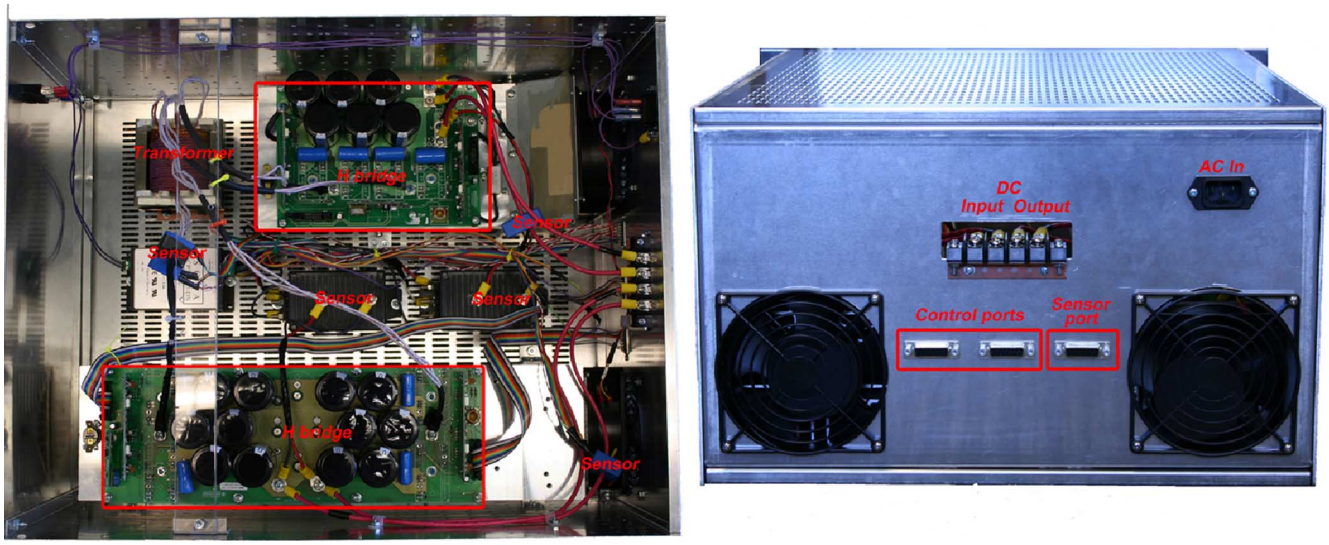

Fig. 3. Full bridge dc/dc converter.

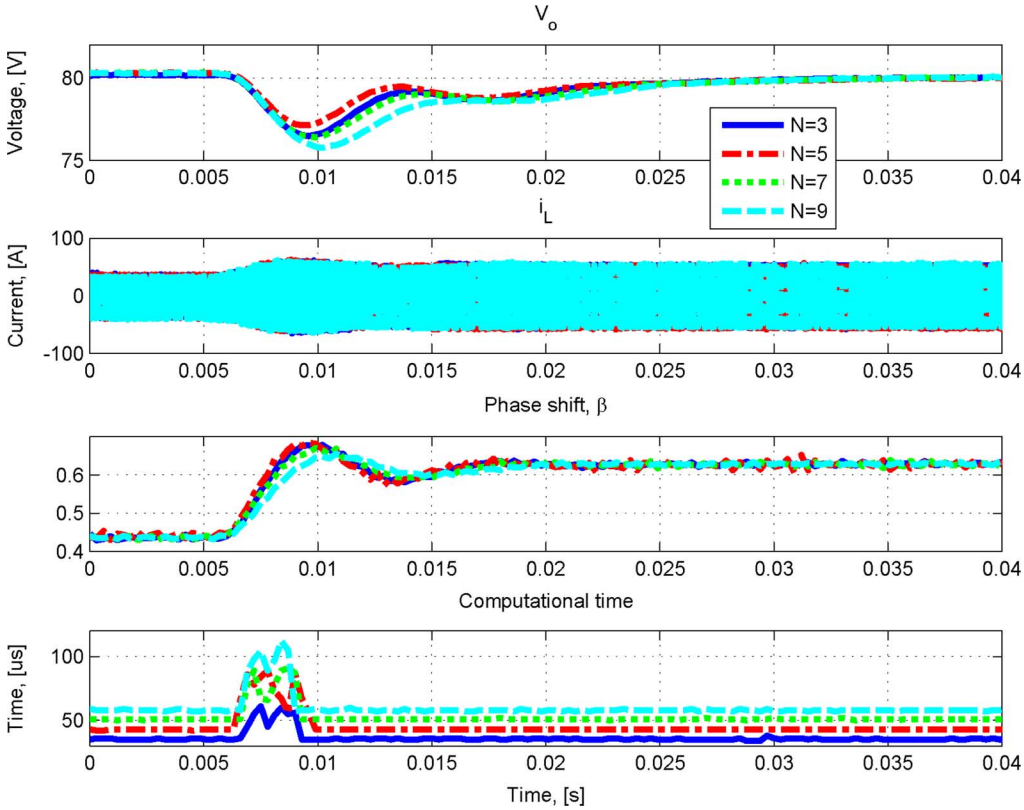

Fig. 4. Performance comparison of LMPC with different prediction horizon for a step-down change of R from 12.8 to 6.4 Ω.

$$V_N(x(k), \mathrm{u}) = \sum_{j=k}^{k+N-1} G(x(j), u(j)) + \Phi(x(N)) \quad (32)$$

subject to

$$x(j+1) = f(x(j), u(j)), \quad f : \mathbb{R}^{n+m} \to \mathbb{R}^n \quad (33)$$
$$x(0) = x(k) \in \mathbb{R}^n \quad (34)$$
$$E(x(\cdot), u(\cdot)) \leq 0, \quad E : \mathbb{R}^{n+m} \to \mathbb{R}^l \quad (35)$$

where

$$\mathrm{u} = \{u(k), u(k+1), \ldots, u(k+N-1)\} \quad (36)$$

is the control sequence

$$\mathrm{x} = \{x(k), x(k+1), \ldots, x(k+N)\} \quad (37)$$

is the state trajectory

$$G(x(j), u(j)) = x(j)^T Q_2 x(j) + u(j)^T W_2 u(j), \quad j = k, k+1, \ldots, k+N-1 \quad (38)$$

and $\Phi(x(N))$ is the penalty for the final states. $Q_2 \in \mathbb{R}^{n \times n}$ and $W_2 \in \mathbb{R}^{m \times m}$ are the corresponding weighting matrices that are used to penalize the deviations of the output and the

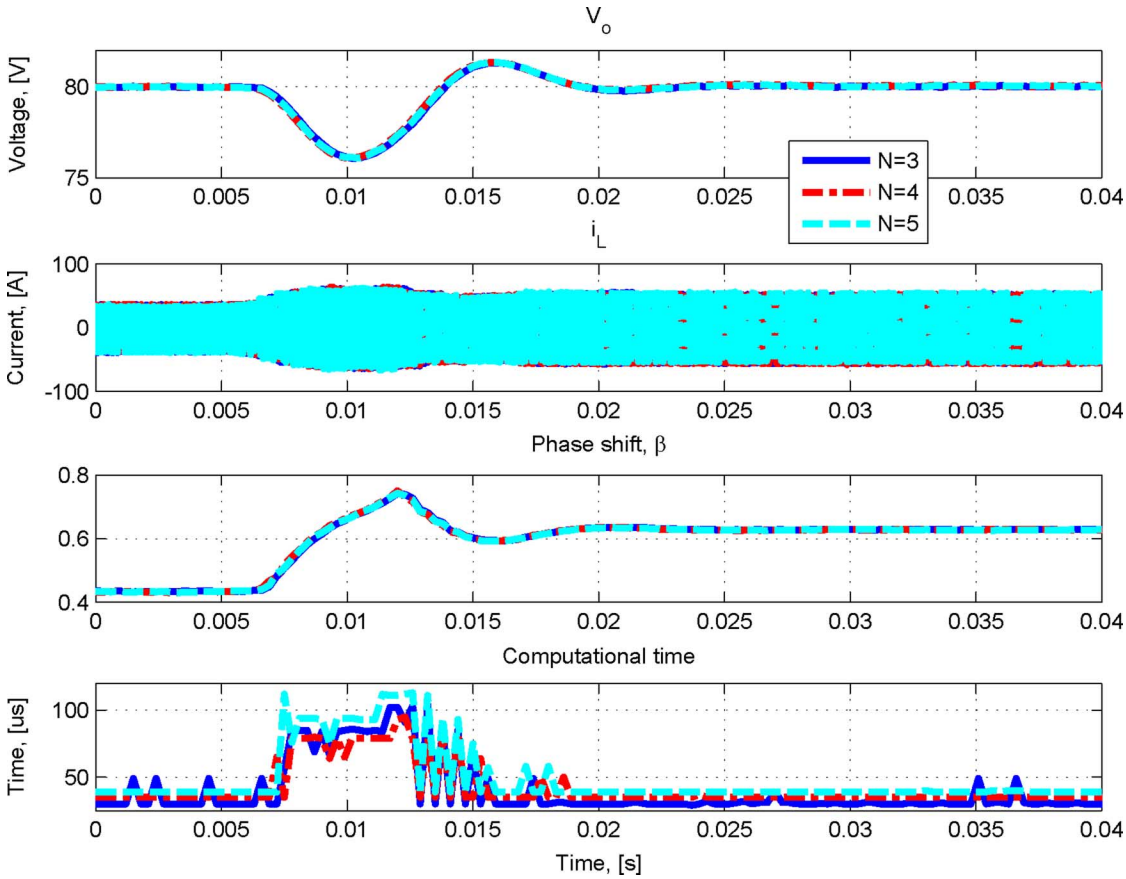

Fig. 5. Performance comparison of NMPC with different prediction horizon for a step-down change of R from 12.8 to 6.4 Ω.

control input from their corresponding desired values, N is the prediction horizon, and $E(x(k), u(k))$ is the constraint matrix and can be written as follows with $l = 3$:

$$\begin{bmatrix} u(j) - 1 \\ -u(j) \\ E_1(x(j), u(j)) \end{bmatrix}. \tag{39}$$

Since the full bridge dc/dc converter has the millisecond level time constant, a rational choice of the sampling time is between 100 and 400 μs [25]. We choose 300 μs as the sampling time for the controller. Moreover, we chose $N \geq 3$ to ensure that the prediction time length is no less than the time constant of the full bridge dc/dc converter. The weighting matrices Q_1, Q_2, W_1, and W_2 are the main tuning parameters of the quadratic cost functions (27) and (38) to shape the closed-loop response for desired performance. The closed-loop performance criteria are defined as: 1) to achieve fast output response with small output overshoot; and 2) to avoid high-frequency control input oscillations that might cause high slew rate for the inductor current and high stress for switching components. If there is high-frequency oscillation for control input, the control input could hit much higher value that leads to higher inductor/power switches current than that of a smooth transient. Although we should be able to choose components to handle the absolute maximum values at phase shift $= 1$, we prefer that the converter operates smoothly during the transient so that phase shift (or equivalently inductor/power switches current) will never hit the highest values. The parameters are selected through simulation using MATLAB/Simulink/SimPowerSystems toolbox based model. The preliminary evaluation results lead to the choice of $Q_1 = [0\,0; 0\,0.01]$, $Q_2 = [0\,0; 0\,0.2]$, and $W_1 = W_2 = 1$. Furthermore, we do not penalize the final states $x(N)$ and $\delta\tilde{x}(N)$, meaning $\Phi(x(N)) = \Phi(\delta\tilde{x}(N)) = 0$. The analysis of stability, though important and interesting, is not covered in the scope of this paper.

Given the fast dynamics of the converter, we employ a method, which we refer to as the InPA-SQP approach [19], [20], to solve the constrained optimization problems for LMPC and NMPC of the full bridge dc/dc converter. The InPA-SQP synergistically combines the solutions derived using perturbation analysis and SQP to solve the optimization problem. It is shown in [19] that it can significantly improve the computational efficiency while effectively handling the nonlinear constraints. Note that, using perturbation analysis or InPA-SQP, one has to assume that a precomputed solution exists and the new solution can be obtained by approximation. When the set point changes, the new optimal solution might be significantly different from the precomputed one. In this case, the InPA-SQP will automatically resort to the SQP algorithm and more iterations might be needed for convergence. However, the same algorithm is still applicable. We now proceed to implement the MPC on our hardware.

V. Experimental Validation

The goal of this section is to present the experimental results to compare the LMPC and NMPC schemes.

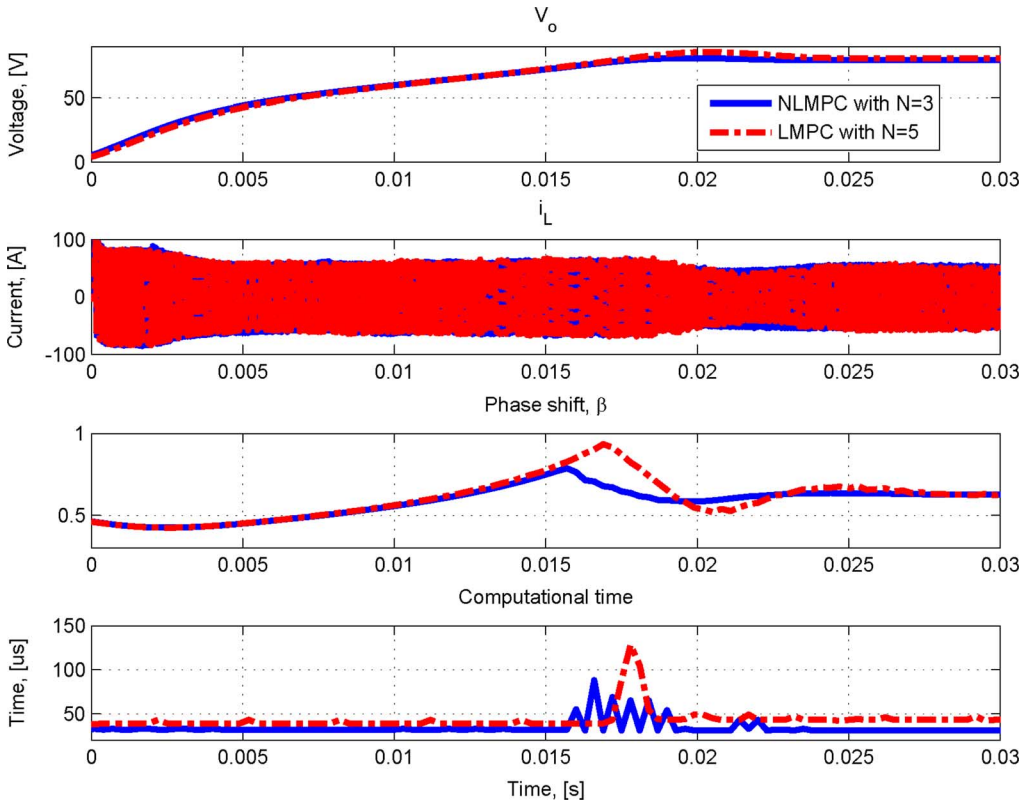

Fig. 6. Comparison of the LMPC and NMPC schemes during the starting process.

Both the LMPC and NMPC schemes are implemented on a full bridge dc/dc converter shown in Fig. 3. The full bridge dc/dc converter is the dc/dc1 of our dc hybrid power system testbed presented in [5]. The dc hybrid power system testbed has multiple unidirectional and bidirectional isolated dc/dc converters as the power conditioning devices and an RT-LAB system as a control rapid prototyping system. The RT-LAB system is a PC which has Xeon 2.8 GHz CPU, 512 MB RAM, and field-programmable gate-array (FPGA)-based I/O cards. Moreover, it runs RedHawk real time operating system. Therefore, it can run compiled code to control those power converters.

Fig. 4 shows the performance of the closed-loop system for LMPC with different prediction horizons N in the presence of a large step change in the load resistance R. Initial R is 12.8 Ω (500 W output power). A step-down change of the load resistance R is then applied to deliver 1000 W output power, which is the rated output power of the converter. The settling times of the LMPC for different prediction horizons N are similar. However, as shown in the first plot of Fig. 4, the transient voltage drop is the smallest when $N = 5$ and $t = 0.009$ s. At both load conditions, the output voltage is regulated to the desired value while the absolute peak value of i_L is less than 75 A for all selected prediction horizons. Therefore, the peak current constraints are not active, which also can be verified by the third plot of Fig. 4. For different prediction horizons, the computational time increases as the prediction horizon increases. It is sometimes believes that the performance of the MPC schemes should improve as the prediction horizon increases. This is not supported by theory and indeed as shown in this paper, the converse can be true. Longer prediction horizons are usually used to ensure that the state enters a terminal set that is used in stability proofs and is not necessarily associated with performance issues. The fact that longer prediction horizon for LMPC does not make any good may be due to inaccuracy of the linear model. More error might be accumulated as prediction horizon increasing. Therefore, a LMPC scheme with long prediction horizon produces control signals such that the nonlinear constraint is satisfied for long future states. However, due to inaccuracy of the model, the decision may be so conservative that even deteriorates the closed-loop performance.

Fig. 5 compares the waveforms for a step-down change of R when the NMPC algorithm with $N = 3, 4$, and 5 is applied to control the power converter. A step-down change of the load resistance R from 12.8 to 6.4 Ω is then applied to deliver 1000 W rated output power. At both load conditions, the output voltage is regulated to the desired value while the absolute peak value of i_L is less than 75 A for all selected prediction horizon. Similar to LMPC, the peak current constraints are not active, which can be verified by the second and third plots of Fig. 5. The performance of NMPC for $N = 3, 4$, and 5 are essentially the same while the computation time increases as the prediction horizon increases. Therefore, it is desirable to choose $N = 3$ to reduce computation time. Note that since the nonlinear model is more accurate that its linear counterparts over a wide operating range of the converter, the NMPC scheme has nondecreasing performance behavior with respect to longer length of horizon.

Fig. 6 shows the experimental waveforms of LMPC and NMPC of the full bridge converter during the starting process with rated 1 kW load. For both the LMPC and NMPC schemes, the peak currents are limited within the maximum tolerable value 75 A for most of the time although the peak current is slightly higher than 75 A during the first 300 μs. The maximum

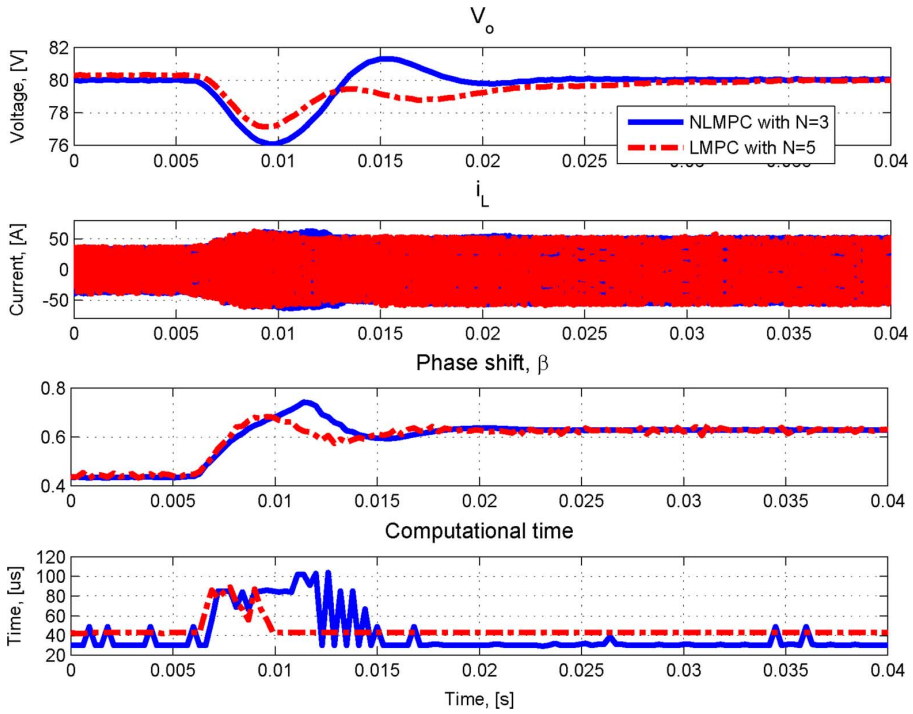

Fig. 7. Comparison of the LMPC and NMPC schemes for a step-down change of R from 12.8 Ω to 6.4 Ω.

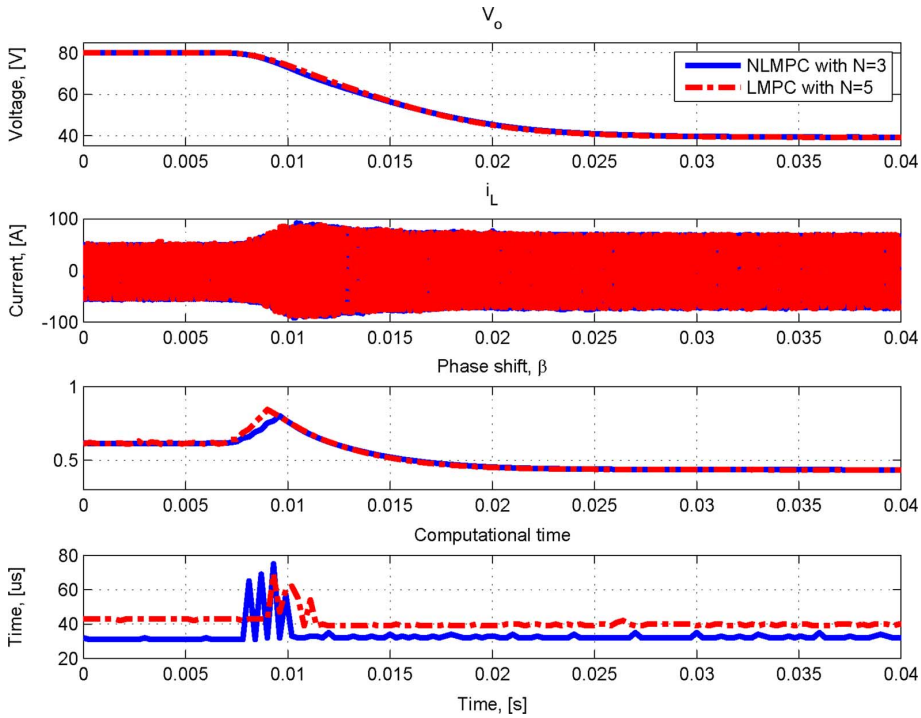

Fig. 8. Comparison of the LMPC and NMPC schemes under overload operation condition.

output voltage is 86 V for the LMPC scheme while, for the NMPC scheme, it is 81.2 V. The maximum computation time for the LMPC scheme is 128 μs which is 40 μs longer than the NMPC scheme's 88 μs. Note that when the active constraint changes to inactive status as indicated on the third plot of Fig. 6, the InPA-SQP algorithm takes more iterations to reach the optimal solution, leading to the additional computation time. For LMPC, in addition to longer prediction horizon, the constraint is active for a longer period of time than that of the NMPC, resulting in much longer computation time. Therefore, for this application, LMPC does not necessarily have shorter computation time than the NMPC scheme.

Fig. 7 shows the waveforms of LMPC and NMPC of the full bridge converter under a step-down change of R. We define the voltage regulation error as $e_v = \int_0^{0.04} |V_o - 80|\, dt$. For the LMPC scheme, $e_v = 0.025$ while for the NMPC scheme, $e_v =$

0.023. Moreover, from Fig. 7 , the settling time of the NMPC scheme is shorter than that of the LMPC scheme. However, the maximum voltage drop of the LMPC scheme is 2.8 V which is 1.1 V lower than that of the NMPC scheme. The maximum computation time for the LMPC scheme is 89 μs while that of the NMPC scheme is 104 μs.

Finally, Fig. 8 shows the experimental waveforms for LMPC and NMPC of the full bridge dc/dc converter under the overload operation condition. The power converter is initially operating with 1 kW load ($R = 6.4\ \Omega$). The load resistance R is then reduced to 2 Ω. For both the LMPC and NMPC schemes, the responses are similar. At the steady state after the transient, the peak current is limited within the maximum tolerable value 75 A except that the peak current is slightly higher than 75 A during the transient. This is partially due to the fact that we do not use a current sensor in the control schemes. The output voltage drops from 80 to 40 V during the transient since i_L is constrained. The maximum computation time for the LMPC scheme is 69 μs which is 6 μs shorter than that of the NMPC scheme.

It is worthwhile to clarify that during our simulation and experimental tests, we did not have feasibility issues. Moreover, we have tested our algorithm with Simulink/SimPowerSystems and Simulink/Embedded MATLAB toolboxes. During those tests, we directly measure all necessary signals without using an observer; the control input hit the constraint curve in the same manner that we observed on experiment tests. We also understood that the control input hit constraint curve because the converter tries to deliver more power, leading to inductor current constraint violation. Furthermore, all of our experimental results show that during the load transient where the set point changes, the computational time is much longer since more iteration is needed for convergence. However, the total computational times at different tests are still much smaller than the sampling time. Therefore, the same algorithm is still applicable.

VI. Conclusion

In this paper, we presented the LMPC and NMPC schemes for the full bridge dc/dc converter under three operating conditions. The experimental results reveal that the MPC algorithms successfully achieved voltage regulation and peak current protection. It is not our intention to compare the two schemes. Instead, it is of interest to report several counterintuitive observations for the two schemes. Those observations suggest that: 1) longer prediction horizon does not guarantee better performance for both linear and nonlinear model-based schemes; and 2) linear model-based scheme does not necessarily have shorter computation time than the nonlinear model-based counterpart.

References

[1] M. H. Kheraluwala, R. W. Gascoigne, D. M. Divan, and E. D. Baumann, "Performance characterization of a high-power dual active bridge dc-to-dc converter," *IEEE Trans. Ind. Appl.*, vol. 28, no. 6, pp. 1294–1301, Nov./Dec. 1992.

[2] D. Fu, F. C. Lee, Y. Qiu, and F. Wang, "Novel high-power-density three-level LCC resonant converter with constant-power-factor-control for charging applications," *IEEE Trans. Power Electron.*, vol. 23, no. 5, pp. 2411–2420, Sep. 2008.

[3] D. Fu, Y. Liu, F. C. Lee, and M. Xu, "Novel driving scheme for synchronous rectifiers in LLC resonant converters," *IEEE Trans. Power Electron.*, vol. 24, no. 5, pp. 1321–1329, May 2009.

[4] Y. Xie, G. Seenumani, J. Sun, Y. Liu, and Z. Li, "A PC-cluster based real-time simulator for all electric ship integrated power systems analysis and optimization," in *Proc. IEEE Electr. Ship Technol. Symp. (ESTS)*, 2007, pp. 396–401.

[5] Y. Xie, J. Sun, C. Mi, and J. S. Freudenberg, "Analysis and modeling of a DC hybrid power system testbed for power management strategy development ," in *Proc. IEEE Veh. Power Propulsion Conf. (VPPC)*, 2009, pp. 926–933.

[6] S. Qin and T. Badgwell, "A survey of industrial model predictive control technology," *Control Eng. Practice*, vol. 11, pp. 733–764, 2003.

[7] D. Q. Mayne, J. B. Rawlings, C. V. Rao, and P. O. M. Scokaert, "Constrained model predictive control: Stability and optimality," *Automatica*, vol. 36, pp. 789–814, Jun. 2000.

[8] M. Morari and J. Lee, "Model predictive control: Past, present and future," *Comput. Chem. Eng.*, vol. 23, pp. 667–682, 1999.

[9] S. Kouro, P. Cortes, R. Vargas, U. Ammann, and J. Rodriguez, "Model predictive control—A simple and powerful method to control power converters ," *IEEE Trans. Ind. Electron.*, vol. 56, no. 6, pp. 1826–1838, Jun. 2009.

[10] A. G. Beccuti, S. Mariethoz, S. Cliquennois, S. Wang, and M. Morari, "Explicit model predictive control of DC-DC switched mode power supplies with extended Kalman filtering," *IEEE Trans. Ind. Electron.*, vol. 56, no. 6, pp. 1864–1874, Jun. 2009.

[11] S. Mariethoz, A. G. Beccuti, and M. Morari, "Model predictive control of multiphase interleaved DC-DC converters with sensorless current limitation and power balance," in *Proc. IEEE Power Electron. Spec. Conf. (PESC)*, 2008, pp. 1069–1074.

[12] T. Geyer, G. Papafotiou, and M. Morari, "Model predictive direct torque control—Part I: Concept, algorithm, and analysis ," *IEEE Trans. Ind. Electron.*, vol. 56, no. 6, pp. 1894–1905, Jun. 2009.

[13] T. Geyer, G. Papafotiou, and M. Morari, "Model predictive direct torque control—Part II: Implementation and experimental evaluation ," *IEEE Trans. Ind. Electron.*, vol. 56, no. 6, pp. 1906–1915, Jun. 2009.

[14] G. Pannocchia and A. Bemporad, "Combined design of disturbance model and observer for offset-free model predictive control ," *IEEE Trans. Autom. Control*, vol. 52, no. 6, pp. 1048–1053, Jun. 2007.

[15] F. Borrelli and M. Morari, "Offset free model predictive control," in *Proc. IEEE Conf. Decision Control*, 2007, pp. 1245–1250.

[16] P. Tøndel, T. A. Johansen, and A. Bemporad, "An algorithm for multi-parametric quadratic programming and explicit MPC solutions," *Automatica*, vol. 39, pp. 489–497, Mar. 2003.

[17] T. Geyer, G. Papafotiou, and M. Morari, "Hybrid model predictive control of the step-down DC-DC converter," *IEEE Trans. Control Syst. Technol.*, vol. 16, no. 6, pp. 1112–1124, Nov. 2008.

[18] Y. Wang and S. Boyd, "Fast model predictive control using online optimization," in *Proc. 17th Int. Federation Autom. Control (IFAC) World Congr.*, 2008, pp. 6974–6997.

[19] R. Ghaemi, J. Sun, and I. Kolmanovsky, "An integrated perturbation analysis and sequential quadratic programming approach for model predictive control," *Automatica*, vol. 45, pp. 2412–2418, Sep. 2009.

[20] R. Ghaemi, J. Sun, and I. Kolmanovsky, "Neighboring extremal solution for nonlinear dicrete-time optimal control problems with state inequality constraints," *IEEE Trans. Autom. Control*, vol. 54, no. 11, pp. 2674–2679, Nov. 2009.

[21] R. Findeisen, F. Allgöwer, M. Diehl, H. Bock, J. Schlöder, and Z. Nagy, "Efficient nonlinear model predictive control," in *Proc. 6th Int. Conf. Chemical Process Control (CPC VI)*, 2000, pp. 454–460.

[22] H. J. Ferreau, H. G. Bock, and M. Diehl, "An online active set strategy to overcome the limitations of explicit MPC," *Int. J. Robust Nonlinear Control*, vol. 18, pp. 816–830, 2007.

[23] F. Borrelli, P. Falcone, T. Keviczky, J. Asgari, and D. Hrovat, "MPC-based approach to active steering for autonomous vehicle systems," *Int. J. Veh. Auton. Syst.*, vol. 3, pp. 265–291, 2005.

[24] J. B. Rawlings and K. R. Muske, "Stability of constrained receding horizon control," *IEEE Trans. Autom. Control*, vol. 38, no. 10, pp. 1512–1516, Oct. 1993.

[25] W. S. Levine, *The Control Handbook*. Boca Raton, FL/Piscataway, NJ: CRC Press and IEEE Press, 1996.